
This is an electronic reprint of the original article.
This reprint may differ from the original in pagination and typographic detail.

Lashkov, Andrey V.; Fedorov, Fedor S.; Vasilkov, Mikhail Yu; Kochetkov, Alexey V.; Belyaev, Ilya V.; Plugin, Ilya A.; Varezhnikov, Alexey S.; Filipenko, Anastasia N.; Romanov, Stepan A.; Nasibulin, Albert G.; Korotcenkov, Ghenadii; Sysoev, Victor V.

The Ti wire functionalized with inherent TiO₂ nanotubes by anodization as one-electrode gas sensor

Published in:
Sensors and Actuators, B: Chemical

DOI:
[10.1016/j.snb.2019.127615](https://doi.org/10.1016/j.snb.2019.127615)

Published: 01/03/2020

Document Version
Peer-reviewed accepted author manuscript, also known as Final accepted manuscript or Post-print

Published under the following license:
CC BY-NC-ND

Please cite the original version:
Lashkov, A. V., Fedorov, F. S., Vasilkov, M. Y., Kochetkov, A. V., Belyaev, I. V., Plugin, I. A., Varezhnikov, A. S., Filipenko, A. N., Romanov, S. A., Nasibulin, A. G., Korotcenkov, G., & Sysoev, V. V. (2020). The Ti wire functionalized with inherent TiO₂ nanotubes by anodization as one-electrode gas sensor: A proof-of-concept study. *Sensors and Actuators, B: Chemical*, 306, Article 127615. <https://doi.org/10.1016/j.snb.2019.127615>

The Ti wire functionalized with inherent TiO₂ nanotubes by anodization as one-electrode gas sensor: a proof-of-concept study

Andrey V. Lashkov¹, Fedor S. Fedorov^{2*}, Mikhail Yu. Vasilkov^{1,3},
Alexey V. Kochetkov¹, Ilia V. Belyaev¹, Ilia A. Plugin¹, Alexey S. Varezhnikov¹,
Anastasia N. Fillipenko¹, Stepan A. Romanov², Albert G. Nasibulin^{2,4},
Ghenadii Korotcenkov⁵, and Victor V. Sysoev^{1*}

¹Yuri Gagarin State Technical University of Saratov, 77 Polytechnicheskaya str., 410054 Saratov, Russia

²Skolkovo Institute of Science and Technology, 3 Nobel str., Moscow, Russia

³Saratov Branch of Kotelnikov Institute of Radioengineering and Electronics of RAS, 38 Zelenaya str., 410019 Saratov, Russia

⁴Aalto University, P.O. Box 16100, 00076 Aalto, Finland

⁵Moldova State University, Mateevici 60, MD-2009 Chisinau, Moldova

Abstract

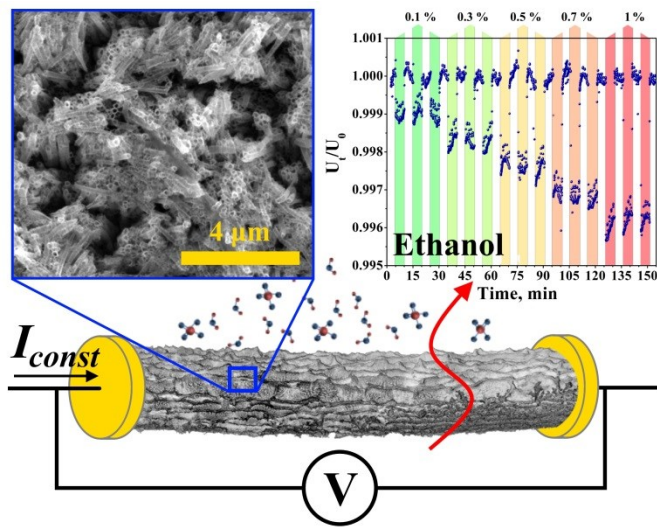
We propose a Ti wire functionalized with inherent anatase TiO₂ nanotubes by an anodization process to serve as a one-electrode gas sensor. The design is similar to other known one-electrode gas sensors when the wire is employed both as a heater and measuring resistive element. We discuss the low-cost fabrication protocol, the structure of the sensor characterized by Raman spectroscopy and electron microscopy, and show the proof-of-concept sensor responses to a few organic vapors, acetone and alcohols, in mixture with air. We have found the response-to-concentration curves to follow a linear fit with a detection limit below 1000 ppm. These findings enlarge the range of possible gas sensor architectures based on nanostructured material for research and practical applications.

Keywords: titanium oxide nanotube; Ti wire; anodization; one electrode; organic vapor; selectivity

*Corresponding author: Tel.: +7-452-998624, Email: vsysoev@sstu.ru (V.S.),

f.fedorov@skoltech.ru (F.F.)

Graphical abstract



Highlights

- New Ti wire-based platform for catalytic and one-electrode sensors has been developed.
- The Ti-TiO₂ nanotube platform is simple and cost-effective to fabricate a gas sensor.
- One-electrode sensors based on Ti wire platform are feasible for detection of organic vapors and development of electronic nose.

1. Introduction

Since the middle of the XX century, gas sensors are utilized for different applications related to monitoring and control of the environment [1] and now are considered as one of integral components in an intelligent engineering [2,3]. For example, according to recent estimations the gas-sensor market is valued to be about \$0.9 billion in 2019 and expected to grow with the rate of 6.2 % up to 2022 [4]. At this market, the catalytic gas sensors, together with other semiconductor ones, occupy about 40 % [4] to be employed in low-cost detectors because of simple design and cost-effective mass-scale production technologies. Still, one-electrode sensors have some advantages over conventional conductometric ones [5] as a low sensor resistance and simplicity of measurement scheme which employs only one power supply [6]. Moreover, the one-electrode gas sensors are considered to exhibit lower sensor resistance's deviations from initial parameter values, i.e. rather a high stability of the initial sensor resistance, that matures from the metal support wire. Therefore, this parameter is not a subject to temporal drift which is often observed in conventional two-electrode metal oxide sensors and allows one eliminating a necessity of frequent sensor calibration. This is quite important issue for example in case of alarm sensors to operate under autonomous conditions.

The fundamental operation principle for catalytic and one-electrode semiconductor sensors which dates back to 60s [7] matures from the sensor resistance change due to adsorption-desorption processes and catalytic reactions at the surface [8, 9]. However, as thoroughly reviewed [5], such sensors have rather limited choice of sensing materials appropriate to be employed for their fabrication. Normally, the sensors are designed with the help of coiled Pt wire encapsulated in a porous dielectric/conductive ceramic bead [10]. The wire serves both as a heating element and as a resistor to be measured under appearance of toxic and flammable gases in an atmosphere. Here, we will show another approach to develop such a one-electrode sensor.

2. The concept of the proposed one-electrode sensor

The basic functioning of catalytic and one-electrode semiconductor sensors implies the metal serving as a support wire should be stable up to approx. 500 °C while the coating where the surface processes are occurred should be porous and have a large active surface area for a free gas access. Moreover, the characteristic dimensions of the fine structures of gas-sensitive material should be comparable with Debye length at the surface region [11,12]. The mentioned requirements are efficiently meet when taking Ti as a basic element. This material is a valve metal whose surface is spontaneously passivated with a pristine dense oxide layer upon exposing to an air environment and is related to the group of refractory metals having melting point of 1670 °C [13]. Recently, there has been reported a technological approach to grow TiO₂ layer in a nanotubular structure by anodization over Ti support which is characterized by a high-aspect ratio and advanced porosity [14,15]. These Ti features allow us to suggest a possible sensor schematically drawn in Figure 1 which can function similar to one-electrode sensor based on Pt wire.

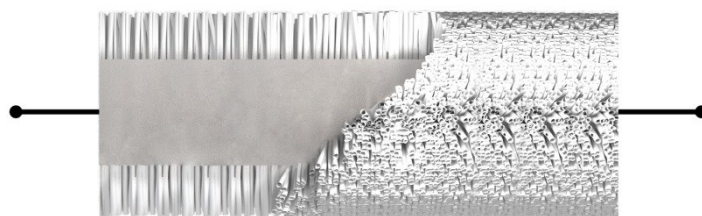


Fig. 1. The concept of new one-electrode sensor based on Ti wire functionalized with inherent TiO₂ NTs.

Here, we explore this concept and show that the anodization of Ti wire is a feasible approach to realize a cost-effective protocol for producing discrete one-electrode gas sensors without employing complex technology operations.

3. Material and Methods

3.1. Preparation and characterization of sensing material

In this study we utilized Ti wires with diameter of ca. 250 μm (99.7%, Sigma-Aldrich, USA) to be anodized in accordance with previously developed protocol [16].

Prior to the anodization we polished the wires at room temperature for 1-2 secs using an etching solution which contained HF (28 %), HNO₃ (30 %), H₂SO₄ (40 %) and CH₃COOH (2 %); all chemicals were of analytical grade. The anodization process was conducted in a two-electrode configuration in the custom-made Teflon® cell, volume of ca. 150 ml, where the wires of 40 mm length were positioned with the help of the commercial terminal sockets (Figure 2). The setup allowed one mounting simultaneously up to eight Ti wires into the same cell as shown in the figure. All the Ti wires were biased at the same positive electric potential as an anode *versus* a stainless steel mesh, area of ca. 100 cm², which served as a cathode. The process was carried out in the electrolyte composed of glycerol (99.5 %) and deionized water (18.2 MΩ) in 3:1 ratio with addition of 0.75 %-mass. ammonium fluoride (98.0 %, Sigma-Aldrich, USA) at a room temperature without steering. We applied a constant voltage of 30 V and acquired the current transient using a lab power supply and multimeter (Keithley 2000), accordingly.

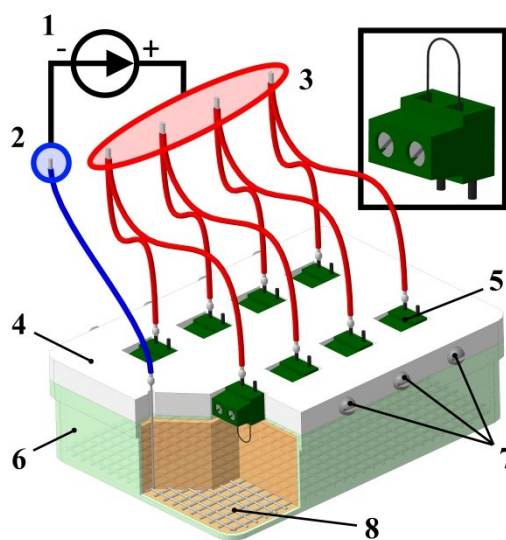


Fig. 2. The experimental setup to grow the TiO₂ NT layer over Ti wires. The positions are, 1 is dc source of constant bias, 2 the negative potential pin (cathode) connection to grid, 3 the positive potential pin to Ti wire, 4 the cover with multiple holes for Ti-wire sockets, 5 the wire sockets, 6 the resistive-plastic container, 7 the fixing screw, 8 the steel grid; the insert shows the single socket with the wire.

The duration of anodization process was up to 80 h. We tested the anodized Ti wire samples obtained at various synthesis times. Following the anodization, the wires

were rinsed with water and then dried for 0.5-2 h at a room temperature. Before assessing gas-sensor properties, we applied a current, up to 500 mA, for 4-10 h to stabilize the oxide layer synthesized over the Ti wire.

To evaluate the morphology of TiO₂ NTs grown over Ti wires under investigation we have employed scanning electron microscopy (SEM) combined with focused ion beam technique (FIB) using Versa 3D (dual beam) microscope (FEI, USA). We sputtered Pt bar of 3x15 μm² over the top of the TiO₂ NTs layer and performed partial etching of the Pt bar by FIB to enable a visualization of the interface which otherwise could be distorted by over- sputtering.

The wire surface was inspected with Raman spectroscopy (DXR™ xi Raman Imaging Microscope, ThermoFisher Scientific, USA) under excitation with a laser, 532 nm wavelength. The laser power was adjusted to be 0.1 mW; we applied an x50 objective. The exposure time was varied in the range of 15-60 s. At least 5 measurements were performed on Ti-TiO₂ NT wires, each in the as-obtained state (just after the anodization) and following an application of dc at 500 mA applied for a thermal stabilization.

3.2. Gas sensor characterization

After the fabrication, the Ti-TiO₂ NT wires housed at two-terminal sockets ([Fig. 1, insert](#)) have been studied as one-electrode sensor prototypes. To carry out the electrical/ gas-sensing measurements we designed the home-made experimental setup employing a gas-flow mode ([Supplemental, Fig. S1](#)). The sensors have been housed to sealed chambers, of ca. 15.5 cm³ volume, equipped with entry and output tubes for gas-flow mode measurement. To feed the setup a lab air was filtered and dried by dry air generator (PG14L, Peak Scientific, UK) in conjunction with a precision compressor (Peak Scientific, UK). The air was forwarded through precise mass-flow controllers (Bronkhorst, Netherlands), yielding the gas flow rate up to 1000 sccm, via bubblers containing the analyte solutions of isopropanol, ethanol and acetone of analytical grade, to come to the gas chambers where one-electrode Ti-TiO₂ NT sensors were

mounted. During the gas-sensor measurements, the analyte solutions were stored at temperature of 30 ± 1 °C to ensure the reported test vapor concentrations within ca. 5 % of error. It is worth noting here that the vapors extracted from the solution into the gas tube could still contain the traces of humidity. We utilized two gas tube lines, for background air and for test vapor emitted from bubblers, which were forked together at the ratio driven by corresponding mass-flow controllers. The ordinary flow rate was 1000 sccm in this study. The vapor concentrations were varied in the range from 0.1 % to 1 %.

The sensors were biased with conventional dc sources (Keithley 2230) and read out by 10-channel multimeter (Keithley 2000) via a 25-pin socket with a rate of 2.07 sec per channel array. All the setup was driven with PC operated under home-made software with the help of the RS-232 interface. The Ti-TiO₂ NT wires were measured in the one-electrode configuration when the dc source is applied along the wire while the voltage dropped along the wire, U , is read out. It is worth noting that we tested in preliminary tests the measuring scheme frequently applied in semiconductor chemiresistors when the sensor element is biased at constant potential in a divider while the current is measured. The differences between the two schemes were minor ones. The gas response of the Ti-TiO₂ NT wire sensor was estimated as

$$S = \frac{\Delta U}{U_0}, \quad (2)$$

where ΔU is the change of dc bias upon the test vapor exposure, U_0 is the dc bias upon the background air exposure. In several preliminary measurements, we varied the operating current in a rather large range, up to 600 mA, and adjusted the optimum one to observe the most prominent chemiresistive effect for each sensor.

The temperature of the Ti-TiO₂ NT wires under Joule heating by passing a current at a gas-sensor operation was estimated with IR-camera (R500EX-P D AVIO/NEC, Nippon Avionics) equipped with macrolense to reach the highest possible spot resolution of 21 μm. To further estimate the temperature and its distribution over the Ti wire under Joule heating during a sensor operation, we have utilized Comsol Multiphysics@5.3a software package under a conjugate gradient iterative solver. The

mesh of the Ti wire in the model included at least 265000 degrees of freedom. The physical model accounted for the material's dependence of electrical conductivity, density, thermal conductivity and heat capacity on the temperature.

4. Results & Discussion

4.1. Anodization of Ti wire

The current transient recorded during anodization of exemplary Ti wire is depicted in the Figure 3. The initial stage of the anodization process is represented by a steep current drop with time (Fig. 2, mark 1) from 30 mA to the values below 0.2 mA because of the growth of compact oxide layer just in accordance to high-field theories [17,18] or other models [19]. The drop is followed by a slight increase of current up to 0.2 mA (Fig. 2, mark 2) around 2 h of anodization time with its further stabilization down to about 0.1 mA with time at ca. 50 h.

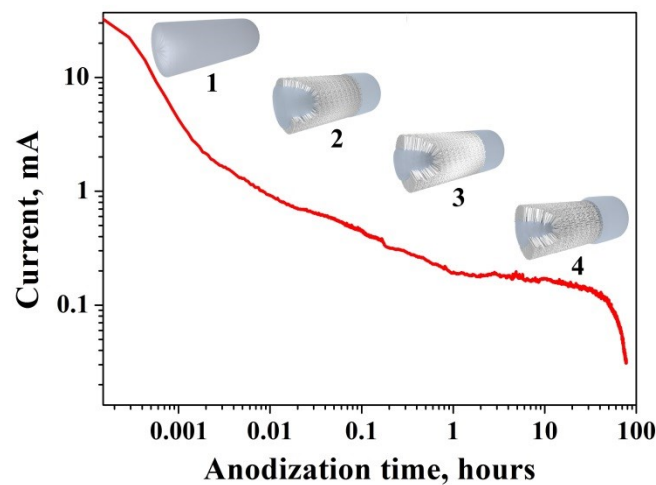


Fig. 3. The change of current with time during the anodization of Ti wire, 250 μm diameter, at application of 30 V potential. The electrolyte is 3:1 gly/ H_2O +0.75% NH_4F solution. See the text for further details.

Such a current behavior is explained by increasing the surface area at the oxidized Ti wire due to the appearance of tubular structure and further balanced interplay between an oxide layer growth and etching [20]. At anodization time of about 50 h (Fig. 3, mark 3) we notice a decrease of current with greater slope which gets to be

more pronounced reaching 70 h (Fig. 3, mark 4). These changes corroborate well with reducing of the oxidized Ti wire diameter which is accompanied by decreasing of its exposed surface as a quadratic function of the wire radius. As we show further in Section 3.2, the wire's anodization process is accompanied by a formation of rather developed meso-nanoporous surface area in the time interval of 40 - 80 h. At the time around 81 h, there is a break of the wire due to mechanical stresses. Therefore, we have not exceeded 80 h of anodization time in our experiments. It is worth noting here that the anodization time could be significantly reduced when taking initial Ti wires of smaller diameter closer to geometry optimal for gas-sensing performance which we discuss in Section 4.3.

4.2. The characterization of Ti-TiO₂ NT wire structure

The SEM inspection of the surface of Ti wire after the anodization reveals an appearance of TiO₂ NT layer where NT mean internal diameter and NT height depend on the anodization time. Using SEM/FIB we have evaluated the geometry of the Ti-TiO₂ NT wires and the appeared nanotubular oxide layer morphology after anodization at various time durations in the range from 15 min to 80 h. Some of exemplary images are collected in Figure 4 to characterize the wires after 15 min, 1 h, 5 h and 60 h of anodization. As one can see, at 15 min of anodization the NTs start to grow from the mesoporous oxide layer and appear to be properly formed at longer anodization time. We have estimated the diameter of the metal core as the difference between overall Ti-TiO₂ NT wire diameter and doubled height of NTs in dependence on the anodization time. The data plotted in Figure 5a show that the Ti core diameter decreases linearly with the anodization time down to 67 μm observed at 80 h of anodization facilitated both by an oxide layer growth and its etching while NTs do not grow linearly with anodization.

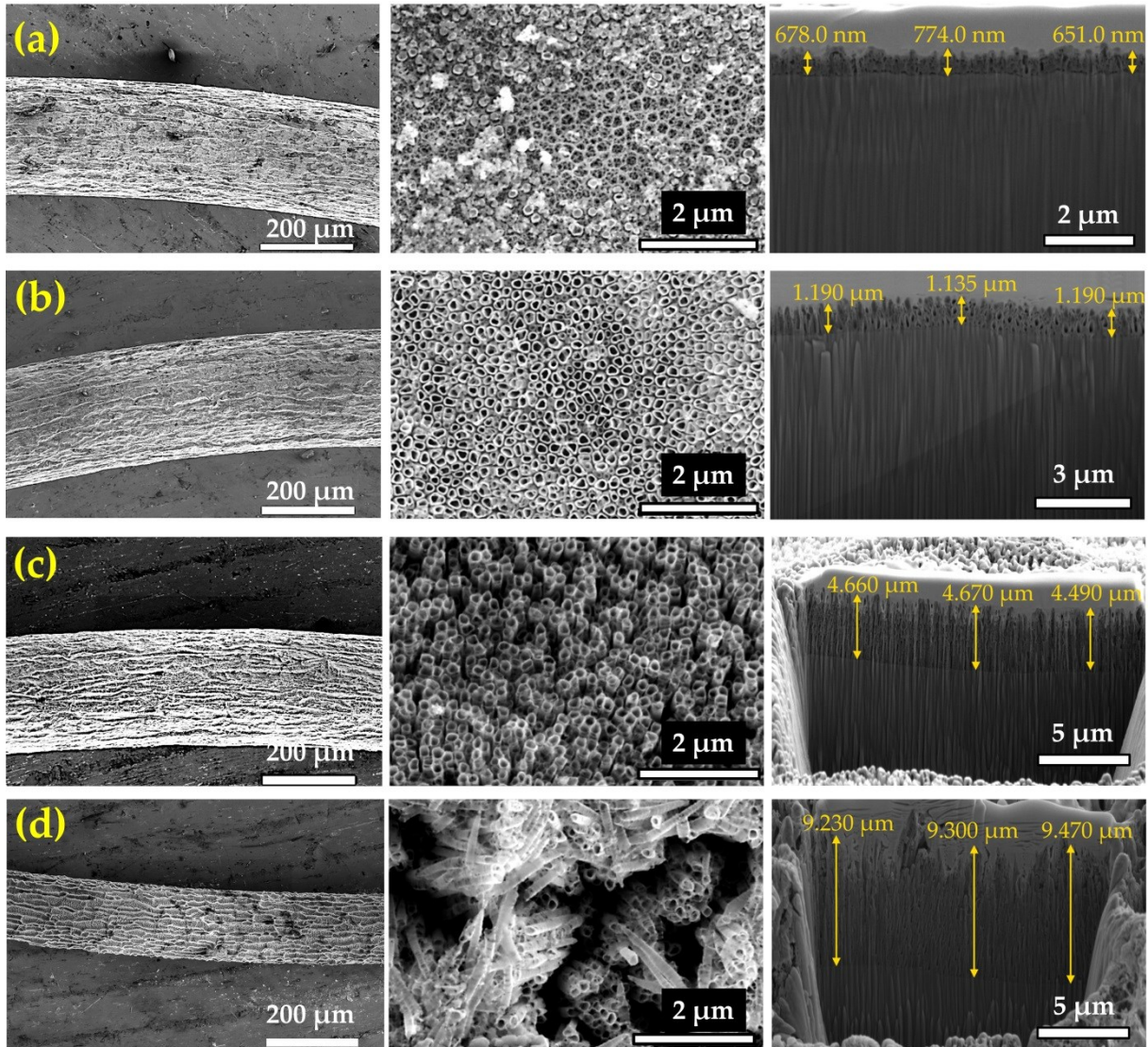


Fig. 4. The SEM images of Ti-TiO₂ NT wire to be the subject of anodization for 15 min (a), 1h (b), 5 h (c) and 60 h (d). Left column are the images of the whole wire, the middle column are the images of the wire surface, the right column are the images of the NT array cross section taken with FIB etching.

Till ca. 10 h of anodization the NTs grow rather linearly from ca. 0.6 μm to ca. 5.3 μm in agreement with other studies [21]. Further, the height still increases with time but much slower to reach ca. 10 μm at 60 h. When matched to the SEM images of Fig. 4 this decrease matures from deviations in NT layer height; the surface appears to be rather developed when anodization time is greater than 50 h. Thus, at long-term anodization the etching process should primarily control the NT layer thickness. The NT internal diameter is rather stable and varies in range of 110-135 nm at different anodization times (Figure 5b) that allows an easy gas access to a total oxide surface.

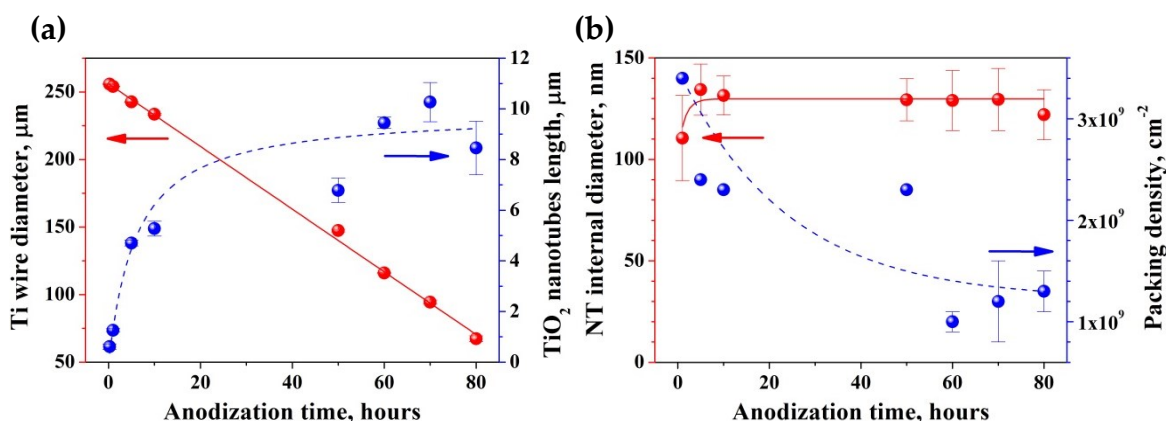


Fig. 5. (a) The dependence of geometry and morphology of the Ti-TiO₂ NT wire on anodization time. (a) Ti core diameter (left y axis), the thickness of oxide layer or a height of NTs (right y axis). The curves are drawn over the experimental data (points) by least squares method as a guide for eyes; (b) NT internal diameter (left y axis) and NT density (right y axis).

Another remarkable feature of NT growth with anodization time is that the NTs appear primarily to be rather dense packed (15 min and 1 h of anodization) and start to diverge at larger duration of anodization time (5 h of anodization) what might be facilitated by etching of the NTs. When the anodization time is about 60 h the NTs tend to form rather separate clusters with large between-in mesopores of up to micron range. Accordingly, the surface density of the NTs at the wire surface goes from ca. $3.4 \cdot 10^9 \text{ cm}^{-2}$ observed after 1 h of anodization to ca. $2.3 \cdot 10^9 \text{ cm}^{-2}$ at 5-50 h of anodization with further reduction down to ca. $1.0\text{-}1.3 \cdot 10^9 \text{ cm}^{-2}$ at 60-80 h of anodization. So, the oxide layer following 60-70 h of anodization is rather dispersed to favor a gas access while the metal core is preserved to be mechanically stable. As a result, we have the structure of the Ti-TiO₂ NT sensor drawn schematically in [Supplemental \(Fig. S4\)](#) which is rather optimal one because, in one hand, it localizes the advanced temperature in the working area under sensor operation and, on the second hand, it ensures appearing side electrical contacts to synthesized Ti NTs that is an imperative condition for current going via the nanotubular oxide layer.

The Raman spectra of the surface of Ti-TiO₂ NT wires, subjected to 60 h anodization, are given in [Figure 6](#). The sample belongs to wires which were found to have optimum gas-sensing performance as discussed in Section 3.3. The red and black

curves drawn in the figure correspond to the as-prepared Ti-TiO₂ NT wire and the wire which was a subject to heating under applied dc equal to 500 mA for 1 h to model the sensor operation, respectively.

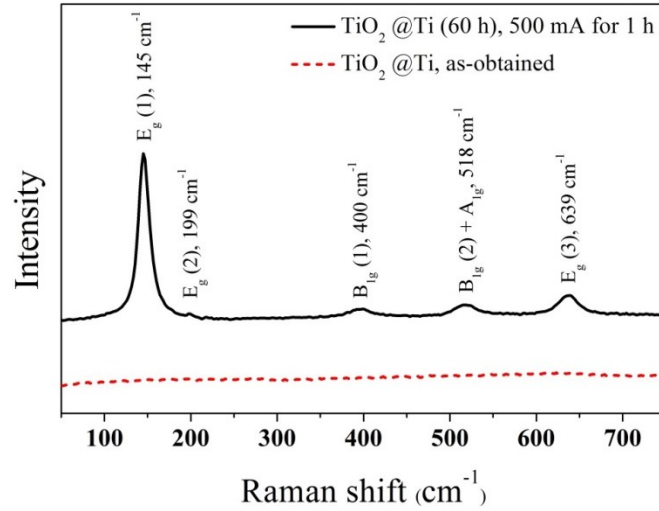


Fig. 6. Raman spectra of the Ti-TiO₂ NT wire surface. Red dotted line corresponds to the sample as-obtained just after the anodization for 60 h, black solid line corresponds to the sample which was a subject to applying the dc current, 500 mA, for 1 h. The peaks are marked according to [22-24].

As one can see, the as-deposited sample does not exhibit any vibration features because the TiO₂ NT layer is amorphous in accordance with other studies [22, 23]. However, heating of the wire results in a crystallization of the oxide NTs that leads to the appearance of six Raman active modes characteristic for anatase which are marked as A_{1g}, B_{1g}(1-2), and E_g(1-3) [24]. The observed bands at 145 cm⁻¹, 199 cm⁻¹ and 639 cm⁻¹ could be assigned to E_g modes while the bands at 400 cm⁻¹ and 518 cm⁻¹ correspond to B_{1g} and A_{1g} modes. Typically for the anatase, the E_g(1) mode is characterized by the higher intensity when compared to other ones. According to Frank et al. [22], A_{1g} appears due to an intrinsic oxygen vibration and B_{1g}(1) mode attributes to intrinsic Ti-atom vibration. The other vibrations, E_g(3), B_{1g}(2) and E_g(1,2), characterize mixes of O- and Ti- atoms motions, Ti-O bond stretching and O-Ti-O bond bending type vibrations, accordingly [23, 24]. So, the Raman spectra ensure the NTs to appear in anatase phase at the wire surface following the Joule heating in a good accordance with our previous observations [25].

4.3. The gas-sensing performance of Ti-TiO₂ NT one-electrode gas sensor

We tested a large number of Ti-TiO₂ NT wires to be a subject of fabrication at different anodization time as discussed in Sections 3.1 and 3.2 upon the exposure to analyte vapors. As noted above, the wires obtained at 80 h of anodization were found to be unstable both in mechanical and electrical/gas-sensing properties. The wires obtained by anodization for the time below 60 h were mechanically stable but required a significant current to activate the chemiresistive effect. Therefore, we employed for gas sensing measurements the wires obtained at 60 h and 70 h of anodization.

The [Figure 7a](#) displays the dependence of response of these two Ti-TiO₂ NT wire one-electrode sensors *versus* isopropanol, 0.1 % concentration, on operating current. As one can see, the currents of around 540 mA and 380 mA are required to observe the maximum magnitude of the sensor response for the wires of 60 h and 70 h of anodization, correspondingly. At this current, the dissipated Joule power, P , lies in a range of 0.6-0.7 W. Since this effect depends primarily on enhancing the wire temperature under Joule heating we tried to find out it with a help of the IR camera. The calibration of the IR camera within the measured geometry range is rather challenging because microscopic defects at any material surface give a significant scatter of the measured temperature. Therefore, we employed two independent ways of the camera calibration. Primarily we have heated the Ti-TiO₂ NT wire and a chromel-alumel thermocouple together at the same hotplate up to 350 °C. In this case, the emission coefficient from the oxidized part of the wire at its middle point was found to be 0.97 to match the thermocouple values in range of 250-350 °C. Secondly, we calibrated the resistance of the Ti-TiO₂ NT wire, R , *versus* a temperature, T , in a thermostatic oven to get the $R(T)$ curve up to 350 °C. Then, we measured the IR radiation from the same wire heated by dc according to sensor operation to be compared with the known $R(T)$ function. In this case, we found the emission coefficient to be equal to approx. 0.6. The noted discrepancy in the emission coefficients reflects a scatter which might appear when measuring such rather small objects where

microscopic defects yield a significant effect. It is still worth noting here that the diameter of these Ti-TiO₂ NT wires, 110-135 μm, is close to the resolution limit of the IR camera. Therefore, the IR camera measurements further account for an interference with surrounding air.

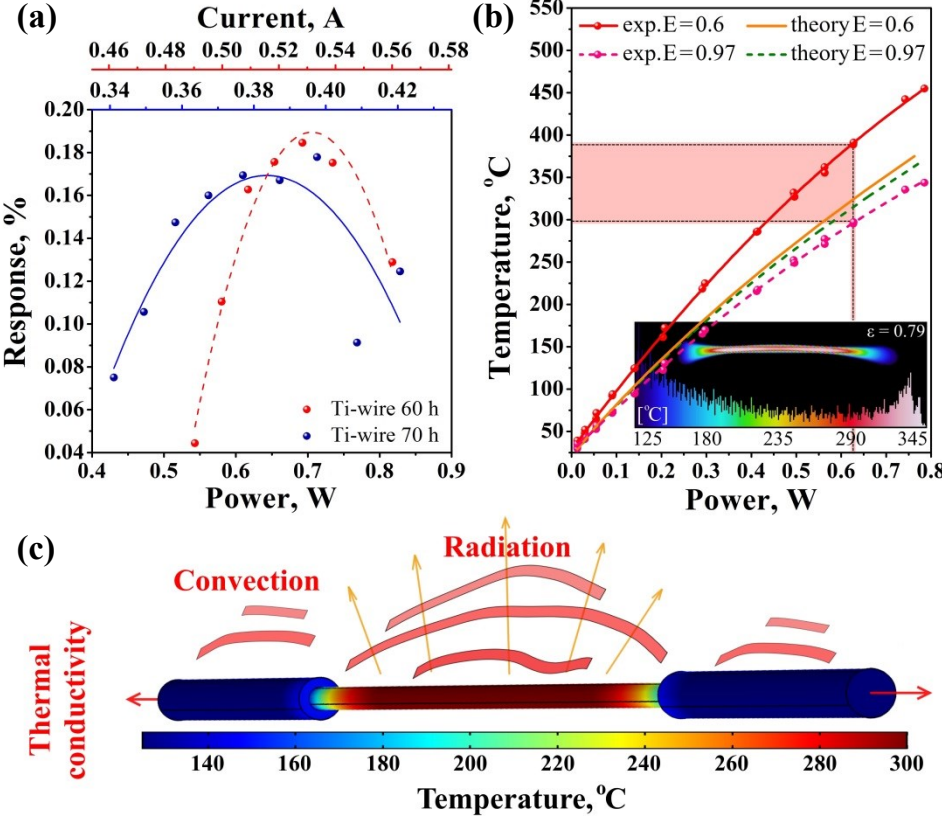


Fig. 7 (a) The effect of operating current/Joule power on the gas response of one-electrode gas sensor based on Ti-TiO₂ NT wire prepared at 60 h and 70 h anodization *versus* isopropanol vapors, 0.1 % concentration, in mixture with background dry air; (b) The effect of Joule power on the temperature of the Ti-TiO₂ NT wire, 60 h of anodization, in lab air conditions measured by IR camera. The points are experimental data measured with IR camera under two emission coefficients, 0.6 and 0.97; dotted lines indicate calculation results with Comsol Multiphysics@5.3a accounting for material emission coefficient equal to 0.6 and 0.97, other parameters are given in the text, insert shows the temperature distribution at pixels in the IR image; (c) the heat pass mechanisms in the Ti-TiO₂ NT wire under operation as the gas sensor.

We have plotted the T(P) dependence, in case for the Ti-TiO₂ NT wire of 60 h anodization, employing IR-camera data recorded at the two values of emission coefficients to define the range of operating temperatures (Figure 7b). The data follow a linear function and the value of P=0.62 W, which was applied under gas sensor tests,

relates to 300-380 °C temperature range. This operating temperature range is further supported by modelling the heating processes in the Ti-TiO₂ NT wire under dc impact using Comsol Multiphysics®. In general, three major processes are responsible for heat dissipation in the wires, including a thermal conductivity from the wires to a metal interface in the socket, convection to environmental gas and an electromagnetic radiation (Figure 7c). For instance, when applying the Joule power to the Ti-TiO₂ NT wire, 60 h of anodization, up to approx. 0.6 W, convection dominates to pass ca. 88 % of the total input power, while ca. 7 % and ca. 5 % dissipate accounting for a radiation and a heat conduction, correspondingly, as detailed in Supplemental. The calculated T(P) curves have agreed with experimental results and show the temperature of ca. 320 °C when the power equal to 0.62 W is applied (Figure 7b). These obtained operating temperatures are similar to ones which we observed when measuring TiO₂ NT array-based multisensor chip to get a chemiresistive effect [25]. However, when compared to pure TiO₂ NTs in one-electrode Ti-TiO₂ NT wires there is a heated metal support core which “shunts” a resistance of the oxide layer. Therefore, the absolute values of gas responses observed here are lower.

Based on these findings, we have tested Ti-TiO₂ NT wires to look for dependence of gas response on analyte vapor concentration. The Figure 8 displays the exemplary $U/U_0(t)$ curves recorded for Ti-TiO₂ NT wire, 60 h anodization, subject of feeding by electrical power equal to 0.62 W, upon an exposure to the three test analyte vapors at various concentrations of 0.1-1 % range. Due to intrinsic limitations for vapor generation using bubblers at room temperature, the isopropanol vapors are given up to 0.7 % while acetone starts from 0.3 % of concentration which, however, do not disturb the experimental trends. As one can see, the measuring U voltage quickly drops down following the analyte appearance according to a reduction of the wire resistance and reversibly returns back to initial value after flushing with dry air. The effect is reversible and reproducible as shown by numerous sequential gas analyte exposures drawn in Fig. 8. Because of rather large gas chamber, where the sensors were mounted, we cannot estimate precisely the response/recovery time but these

characteristic times are less than 10 sec to be comparable to that of atmosphere change within the sealed chamber.

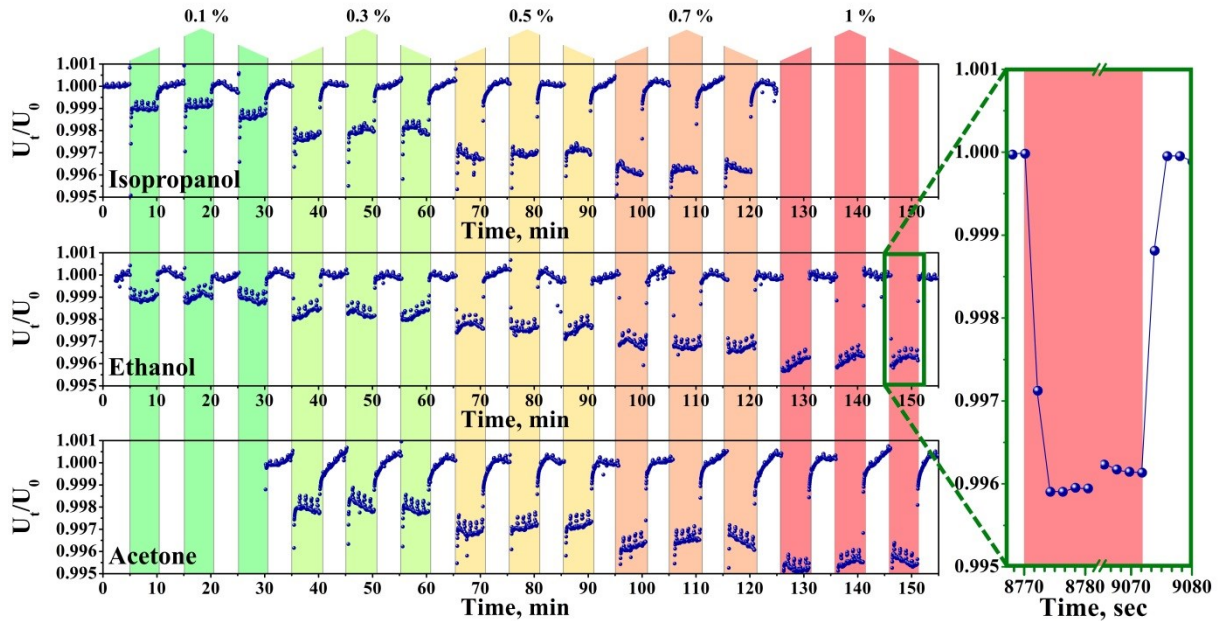


Fig. 8. The change of measuring voltage during the operation of Ti-TiO₂ NT wire-based one-electrode sensor upon exposure to three vapor analytes, isopropanol, ethanol, acetone, at various concentrations, 0.1-1 %, in a mixture with the background air. The data are given for exemplary sensor fabricated at 60 h of Ti wire anodization under application of 0.62 W electrical power.

The analytical signal of voltage change exceeds the magnitude of the experimental noise even at 0.1 % concentration of vapor concentrations. These data are comparable to extensively studied carbon-derived nanostructures like nanotubes or graphene [26]. The higher analyte concentrations produce more pronounced effect. For example, we have drawn the dependence of gas response of Ti-TiO₂ NT wire, 60 h of anodization, on analyte concentrations in Figure 9. All the curves follow a linear function which is an inherent advantage of one-electrode sensors in agreement with other reports dealing with SnO₂ [27, 28] and In₂O₃ [29, 30] sensing materials. The observed differences in the response to different analytes could relate to surface chemistry (receptor function) and reflect an exchange between local states in the gap and conductance band of TiO₂ as well as to free carrier diffusion along/into the meso-nanoporous oxide layer (transduction function).

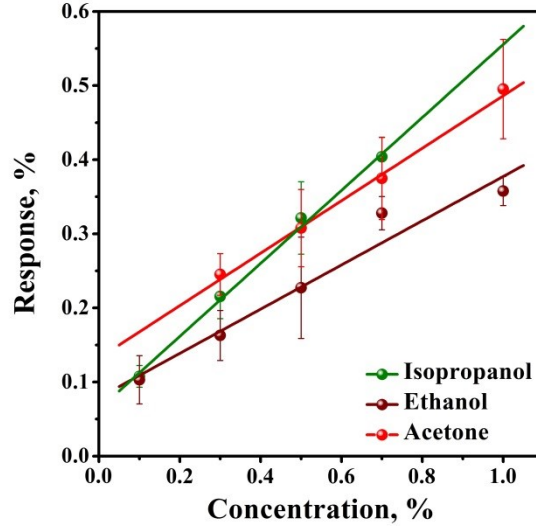


Fig. 9. The response-to-analyte concentration dependence of one-electrode sensor based on Ti-TiO₂ NT wire, 60 h of anodization. The analytes are isopropanol, ethanol and acetone at 0.1-1 % concentration range in mixture with a background dry air.

These observations ensure that the developed one-electrode Ti-TiO₂ NT sensors have sensitivity appropriate for in-practice detection of alcohols. However, the single sensor responses are not selective enough to distinguish the test analytes. To approach it, we have employed the concept of e-nose which considers combining sensors with diverse characteristics into an array [31] and further vector signal processing by pattern recognition techniques [32].

For differentiating the properties of the developed one-electrode sensors we have considered a time of anodization which is the most influential parameter for the sensor fabrication as discussed above. The e-nose multisensor array tested here have been composed of minimum number of three one-electrode sensors based on Ti-TiO₂ NT wires, two prepared at 60 h of anodization and one prepared at 70 h of anodization, which were exposed simultaneously to organic vapor analytes. The Figure 10 (a-c) shows the distribution of sensor responses in this rudimentary multisensor array *versus* to three analytes. As one can see, the distributions are specific to vapor kind that allows one its selective recognition.

The generated array vector signal has been processed by linear discriminant analysis (LDA) as detailed in our previous works (see, for instance, [33, 34]). In brief,

this technique transfers the primary vector signal recorded for different classes of measurements into another coordinate system where these vectors could be distinguished to a maximum degree via optimizing a ratio of between-class variation of vector signals to their in-class dispersion [35].

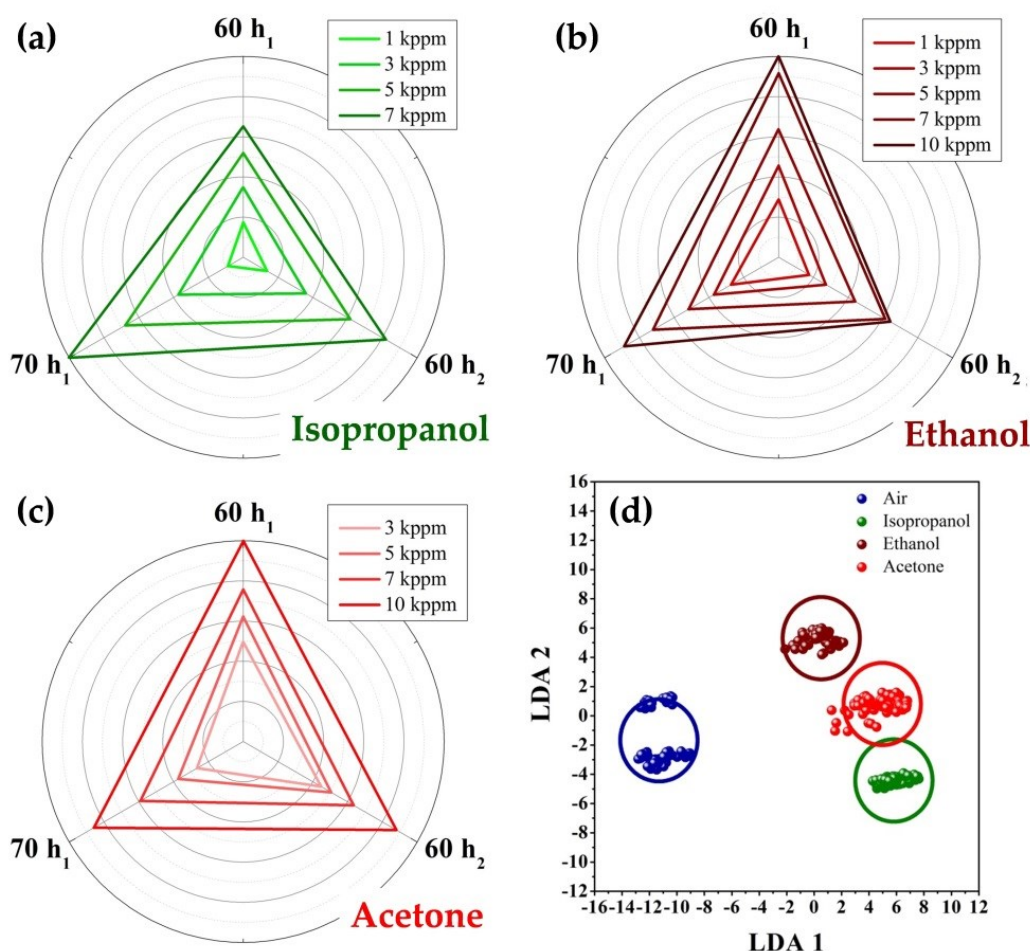


Fig. 10. (a-c) The vector signal of multisensor array consisted of three one-electrode sensors based on Ti-TiO₂ NT wires, 60 h (60 h₁ and 60 h₂) and 70 h (70 h₁) of anodization exposed to three vapor analytes, isopropanol (a), ethanol (b) and acetone (c), the sensor responses are normalized to maximum values for clarifying “sensor patterns” of the vapors; (d) LDA processing of the vector signals to three organic vapors of 0.7 % concentration. The circles are built around cluster gravity centers with 0.95 confidence level while the points are experimental signals.

Figure 10d shows the vector signals of our array of one-electrode sensors based on Ti-TiO₂ NT wires to vapor analytes, 0.7 % concentration, being processed by LDA to project into a coordinate system of first two LDA components. As one can see, the

vector signals to various analytes are grouped at well-separate areas of the LDA space. The possession of points to classes is defined by circles built with 0.95 confidence level around the classes' gravity centers. The most of experimental vector points fall into the defined classes which allow one recognizing the vapor analytes even with such a rudimentary multisensor array.

4. Conclusion and future work

We have tried out the protocols to design one-electrode sensors based on Ti wires with TiO₂ NTs at high-aspect ratio which is different to ones based on noble metals and tested the sensor performance *versus* organic vapors in sub-percent concentration range. An inherent property of the developed sensors is the linearity of sensor response with gas concentration which could be detected at least down to 0.1 %. To further advance the sensor characteristics the bridge electronic circuits when two and more sensors are combined could be employed.

The considered Ti-wire platform has been studied as a one-electrode sensor where the chemiresistive effect dominates. Nevertheless, there are opportunities to perform a catalytic sensor by the wire surface modification via the known catalysts which promote a catalytic oxidation of flammable gases. In this case, the effect of temperature modulation in the working area will play a significant role. Altogether, the suggested technology is characterized by extreme simplicity which does not require a complicated equipment that makes it favorable when compared to known conventional routes to produce gas sensors. Since the suggested fabrication protocol of the Ti-TiO₂ NT sensors is compatible with planar technologies they could be further explored in frames of MEMS technologies, also in terms of long-term stability.

Acknowledgments

The authors thank Russ. Ministry of Education and Science for a partial support by grant no. 16.1119.2017/4.6. F.S.F. and S.R. thank Russian Science Foundation for support of SEM/FIB and Raman spectroscopy studies by grant no. 19-72-00136. Research of G.K. was supported by the State Program of the Republic of Moldova, project 15.817.02.29F.

References

1. N. Barsan, K. Schierbaum (Eds.), Gas Sensors Based on Conducting Metal Oxides: Basic Understanding, Technology and Applications, Elsevier, 2018, 292 pp. <https://doi.org/10.1016/C2016-0-00984-1>.
2. R. A. Potyrailo, Toward high value sensing: monolayer-protected metal nanoparticles in multivariable gas and vapor sensors, *Chem. Soc. Rev.* 46 (2017) 5311. <https://doi.org/10.1039/c7cs00007c>.
3. A. Lewis, P. Edwards, Validate personal air-pollution sensors, *Nature* 535 (2016) 29-31. <https://doi.org/10.1038/535029a>.
4. E. Mounier, B. Roussel, Gas and Particle Sensors 2018, Market & Technology Report, Yole Développement, November 2018. <https://www.i-micronews.com/products/gas-and-particle-sensors-2018/>.
5. G. Korotcenkov, Practical aspects in design of one-electrode semiconductor gas sensors: status report, *Sensors and Actuators B* 121 (2007) 664–678. <https://doi.org/10.1016/j.snb.2006.04.092>.
6. S. P. Lee, Electrodes for semiconductor gas sensors, *Sensors* 17 (2017) 683. <https://doi.org/10.3390/s17040683>.
7. A. R. Baker, Improvements in or relating to electrically heatable filaments, Patent GB892530, 1962.
8. K. Komatsu, S. Sakai, K. Fukui, Gas sensor, Patent EP0115953, 1984.
9. S. N. Malchenko, I. N. Lychkovsky, M. V. Baykov, One-electrode semiconductor sensors for detection of toxic and explosive gases in air, *Sensors and Actuators B* 7 (1992) 505-506. [https://doi.org/10.1016/0925-4005\(92\)80353-Y](https://doi.org/10.1016/0925-4005(92)80353-Y).
10. S. J. Gentry, T. A. Jones, The role of catalysis in solid-state gas sensors, *Sensors and Actuators* 10 (1986) 141-163. [https://doi.org/10.1016/0250-6874\(86\)80039-7](https://doi.org/10.1016/0250-6874(86)80039-7).
11. V. V. Kissine, V. V. Sysoev, S. A. Voroshilov, Individual and collective effects of oxygen and ethanol on the conductance of SnO₂ thin films, *Applied Physics Letters* 76 (2000) 2391-2393. <https://doi.org/10.1063/1.126381>.
12. A. Rothschild, Y. Komem, The effect of grain size on the sensitivity of nanocrystalline metal-oxide gas sensors, *Journal of Applied Physics* 95 (2004) 6374-6380. <https://doi.org/10.1063/1.1728314>.
13. F. Habashi, Historical introduction to refractory metals, *Mineral Processing and Extractive*

- Metallurgy Review 22 (2001), 25–53. <https://doi.org/10.1080/08827509808962488>.
14. D. Gong, C. A. Grimes, O. K. Varghese, W. Hu, R. S. Singh, Z. Chen, E. C. Dickey, Titanium oxide nanotube arrays prepared by anodic oxidation, *J. Mater. Res.* 16 (2001) 3331–3334. <https://doi.org/10.1557/JMR.2001.0457>.
 15. J. M. Macak, H. Tsuchiya, P. Schmuki, High-aspect-ratio TiO₂ nanotubes by anodization of titanium, *Angewandte Chemie Int. Ed.* 44 (2005) 2100–2102. <https://doi.org/10.1002/anie.200462459>.
 16. M. Y. Vasilkov, F. S. Fedorov, N. M. Ushakov, S. Y. Suzdaltsev, Field electron emission from titanium dioxide nanotubes, *Tech. Phys. Lett.* 41 (2015) 29–31. <https://doi.org/10.1134/S1063785015010149>.
 17. E. J. W. Verwey, Electrolytic conduction of a solid insulator at high fields: the formation of the anodic oxide film on aluminium, *Physica* 2 (1935) 1059–1063. [https://doi.org/10.1016/S0031-8914\(35\)90193-8](https://doi.org/10.1016/S0031-8914(35)90193-8).
 18. N. Cabrera, N. F. Mott, Theory of the oxidation of metals. *Reports on Progress in Physics* 12 (1949) 163–184. <https://doi.org/10.1088/0034-4885/12/1/308>.
 19. A. Güntherschulze, H. Betz, Die Elektronenströmung in Isolatoren bei extremen Feldstärken, *Zeitschrift Für Phys.* 91 (1934) 70–96. doi:10.1007/BF01340550.
 20. P. Roy, S. Berger, P. Schmuki, TiO₂ nanotubes: synthesis and applications. *Angew. Chemie Int. Ed.* 50 (2011) 2904–2939.
 21. C. A. Grimes, G.K. Mor, *TiO₂ Nanotube Arrays: Synthesis, Properties, and Applications*, Springer: Dordrecht, Heidelberg, London, New York (2009) 1–345.
 22. O. Frank, M. Zikalova, B. Laskova, J. Kürti, J. Koltai, L. Kavan, Raman spectra of titanium dioxide (anatase, rutile) with identified oxygen isotopes (16, 17, 18), *Phys. Chem. Chem. Phys.* 2012, 14, 14567–14572. <https://doi.org/10.1039/C2CP42763J>.
 23. A. Niilisk, M. Moppel, M. Pärns, I. Sildos, T. Jantsonm, T. Avarmaa, R. Jaaniso, J. Aarik, Structural study of TiO₂ thin films by micro-Raman spectroscopy, *Cent. Eur. J. Phys.* 4 (2006) 105–116. <https://doi.org/10.1007/s11534-005-0009-3>.
 24. T. Ohsaka, F. Izumi, Y. Fujiki, Raman spectrum of anatase, TiO₂, *J. Raman Spectrosc.* 7 (1978) 321–324. <https://doi.org/10.1002/jrs.1250070606>.
 25. F. Fedorov, M. Vasilkov, A. Lashkov, A. Varezhnikov, D. Fuchs, Ch. Kübel, M. Bruns, M. Sommer, V. Sysoev, Toward new gas-analytical multisensor chips based on titanium oxide nanotube array, *Scientific Reports* 7 (2017) 9732. <https://doi.org/10.1038/s41598-017->

- 10495-8.
26. V. Schroeder, S. Savagatrup, M. He, S. Lin, T.M. Swager, Carbon nanotube chemical sensors, *Chem. Rev.* 119 (2019) 599–663. <https://doi.org/10.1021/acs.chemrev.8b00340>.
 27. D. R. Orlik, M. I. Ivanovskaya, G. A. Branitsky, P. A. Bogdanov, Mono-electrode gas sensors based on SnO₂ semiconductor ceramics, *Sensors and Actuators B* 13-14 (1993) 605-607. [https://doi.org/10.1016/0925-4005\(93\)85111-M](https://doi.org/10.1016/0925-4005(93)85111-M).
 28. K.-D. Song, B.-S. Joo, N.-J. Choi, Y.-S. Lee, S.-M. Lee, J.-S. Huh, D.-D. Lee, A micro hot-wire sensors for gas sensing applications, *Sensors and Actuators B* 102 (2004) 1–6. <https://doi.org/10.1016/j.snb.2003.11.038>.
 29. S. N. Malchenko, I. N. Lychkovsky, M. V. Baykov, In₂O₃-based gas sensors, *Sensors and Actuators B* 7(1992) 505-506. [https://doi.org/10.1016/0925-4005\(93\)85350-J](https://doi.org/10.1016/0925-4005(93)85350-J).
 30. G. Korotcenkov, I. Boris, V. Brinzari, V. Golovanov, Yu. Lychkovsky, G. Karkotsky, A. Cornet, E. Rossinyol, J. Rodrigue, A. Cirera, Gas-sensing characteristics of one-electrode gas sensors based on doped In₂O₃ ceramics, *Sensors and Actuators B* 103 (2004) 13–22. <https://doi.org/10.1016/j.snb.2004.02.016>.
 31. K. Persaud, G. Dodd, Analysis of discrimination mechanisms in the mammalian olfactory system using a model nose. *Nature* 299 (1982) 352-355. DOI: 10.1038/299352a0
 32. J. W. Gardner, P. N. Bartlett, A brief history of electronic noses. *Sensors & Actuators B* 18 (1994) 211 – 221. DOI: 10.1016/0925-4005(94)87085-3
 33. V. V. Sysoev, I. Kiselev, M. Frietsch, J. Goschnick, The temperature gradient effect on gas discrimination power of metal-oxide thin-film sensor microarray, *Sensors* 4 (2004) 37-46. <https://doi.org/10.3390/s40400037>.
 34. V. V. Sysoev, I. Kiselev, V. Trouillet, M. Bruns, Enhancing the gas selectivity of single-crystal SnO₂:Pt thin film chemiresistor microarray by SiO₂ membrane coating, *Sensors and Actuators B* 185 (2013) 59-69. <https://doi.org/10.1016/j.snb.2013.04.087>.
 35. A. Hierlemann, R. Gutierrez-Osuna, Higher-order chemical sensing, *Chem. Rev.* 108 (2008) 563–613. <https://doi.org/10.1021/cr068116m>.